Supplemental Document for

Computational Design of Metallophone Contact Sounds

Gaurav Bharaj[*] David I.W. Levin[†] James Tompkin[*] Yun Fei[‡] Hanspeter Pfister[*] Wojciech Matusik[§] Changxi Zheng[‡]

[*] Harvard Paulson SEAS [†] Disney Research [‡] Columbia University [§] MIT CSAIL

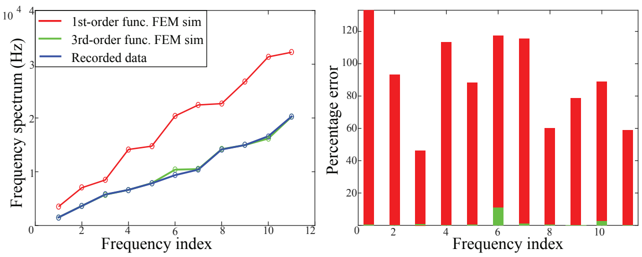

Figure 1: *A comparison of the accuracy of 1^{st} and 3^{rd} order tetrahedral finite elements for modal sound simulation for a shape. On the left is comparison of 1^{st}, 3^{rd}-order vs recorded data, while on the right is 1^{st} and 3^{rd} percentage error vs. recorded data.*

1 Higher-Order FEM for Fabrication

Accurate simulation is critical for sound design problems. Even a frequency error of a few percent can impact the perceived quality of the results. No matter how robust our optimization scheme, it can be doomed to failure if simulation results do not match real-world outcomes. Many fabrication algorithms in computer graphics rely on linear (referring to the shape function order) tetrahedral finite elements to predict the physical behavior of design instances (e.g., in Bickel et al. [2010]). However, such finite elements are well-known to be extremely inaccurate; worse yet, they do not approach the correct solution value even as the simulation discretization is refined [Hughes 2012]. In this paper we rely on 3^{rd} and 4^{th} order finite elements via COMSOL [2005]. COMSOL also performs online remeshing in order to guarantee solution quality. However, even in the presence of this remeshing scheme experimental evidence (Figure 1) shows that the results produced by our algorithm would not be possible without higher-order finite elements.

2 Fabrication and Materials

With optimized geometry in hand, we turn our attention to fabrication. Most struck idiophones are fabricated in wood or metal, as plastics produce dull sounds. While wood produces a rich sound, especially with a resonating chamber as in a marimba, it is difficult to work with as the material density and stiffness vary between pieces due to structural differences (e.g., fiber arrangement and knots).

This leaves metal: Modern CNC tools can accurately and automatically reproduce our geometries. All 2D examples in this paper were produced by water jetting Aluminum 6063-T83. Our 3D examples were, geometry permitting, produced using CNC milling of Aluminum 6063-T83; otherwise, we relied on 3D printing from a commercial vendor [Sha]. Table 1, shows the material properties of all fabrication materials and outlines which process was used to manufacture each example.

Material Calibration. Correct simulation of sound spectra requires an accurate Young's Modulus and Poisson's Ratio. Shapeways' metal 3D printing process uses the Stainless-Steel 420 SS + Bronze alloy. Though its material properties are documented online, we chose to validate the specifications ourselves. Inspired by Bickel et al. [2009], we optimize for material properties so that the simulated frequency spectrum matches a recording of a real material sample (Figure 2).

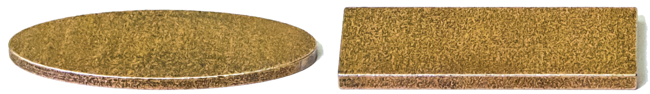

Figure 2: *3D printed geometry used for Shapeways material calibration.*

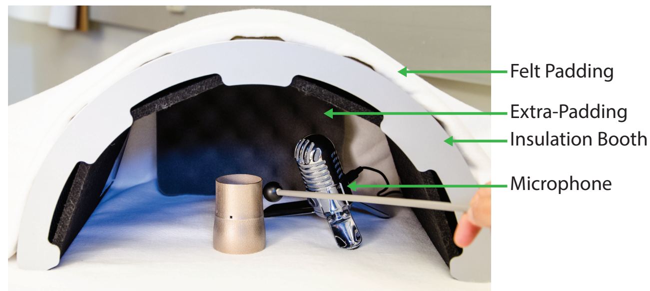

Figure 3: *Measurement is conducted inside an isolation booth (shown open), here provided by an sE SPACE reflection filter.*

We solve this inverse problem using our contact sound design method, with one change. Rather than choosing the design map parameters, $\boldsymbol{p}$, to be geometry modifications or perforations, we choose them to be the Young's Modulus and Poisson's Ratio of the object's material. Validation was performed by simulating the sound spectra of an unmeasured object and comparing it to a real-world recording. Finally, we compared our computed values against vendor-supplied material parameters, yielding an error of 1%. We found that our optimized material properties produced more accurate results than those provided by Shapeways, and therefore we used them for all relevant experiments.

3 Sound Measurement

This quantitative error must be measured, but this is complex: our optimizations are surrounding-environment-free, but our recording environment is not. One option would be to try to simulate our real world environment, as per [O'Brien et al. 2002], but this is complex and error prone. Instead, we try to isolate our samples from the real world. The goal here is to prevent sound leaving the piece, reflecting in the real world, and returning distorted to the microphone (Samson Meteor). As such, we use a reflection filter as an isolation booth (Fig.3), and surround it with dense fabrics. Finally, to reliably strike pieces with consistent force while inside the covered booth, we build a robotic mallet from a striking solenoid and an Arduino.

Example	Metal-Name	Fabrication-Method	Young's-Modulus (Pa)	Poisson's-Ratio	Density (Kg/m^3)
Zoolophone	Aluminum 6063-T83	Water-jetting	$6.9e10$	0.33	2700
City-Scale	Aluminum 6063-T83	CNC-Milling	$6.9e10$	0.33	2700
3D-Cups	Stainliess-Steel 420 SS+ Bronze	3D-Printing	$1.48e11$	0.32	8093

Table 1: *Material properties and fabrication methods for all examples.*

4 Derivatives of the General Eigenvalues

To aid explanation, we reproduce the key equations (2, 3, 4, and 5) from the main paper. The linear modal analysis equation:

$$\mathsf{KU} = \mathsf{MUS} \text{ and } \mathsf{U}^T\mathsf{MU} = \mathsf{I}. \tag{1}$$

The frequency and amplitude estimation equation:

$$\omega_i = \frac{1}{2\pi}\sqrt{\mathsf{S}_{i,i}} \text{ and } a_i = |\boldsymbol{f}^T\boldsymbol{u}_i|, \;\; i = 1...N, \tag{2}$$

The frequency composition objective function equation:

$$E_\omega(\boldsymbol{p}) = \sum_{k\in\mathcal{K}_f} \frac{w_k}{\omega_k^*}\left[\omega_k(\phi(\boldsymbol{p})) - \omega_k^*\right]^2, \tag{3}$$

The frequency amplitude objective function equation:

$$E_a(\boldsymbol{p}) = \sum_{k\in\mathcal{K}_a} \frac{w_k}{\bar{a}_1}\left[a_k(\phi(\boldsymbol{p})) - a_k^*\right]^2, \tag{4}$$

Quasi-Newton methods such as the SQP require evaluating the derivative of the objective function, which in our case amounts to evaluating the derivative of eigenvalues with respect to each parameter. The derivative of Equation (3) over the j-th parameter is:

$$\frac{\partial E_\omega}{\partial p_j} = \frac{1}{2\pi}\sum_{k\in\mathcal{K}_f}\frac{w_k}{\omega_k^*}\left(\frac{1}{2\pi} - \frac{\omega_k^*}{\sqrt{\lambda_k}}\right)\frac{\partial\lambda_k}{\partial p_j}, \tag{5}$$

where λ_k is the object's k-th vibration mode (i.e., $\lambda_k = \mathsf{S}_{k,k}$ in Equation (2)). Calculating the derivative $\frac{\partial\lambda_k(p_j)}{\partial p_j}$ for the k-th eigenvalue λ_k is nontrivial. Based on [de Leeuw 2007], we take the derivative of $\mathsf{K}\boldsymbol{u}_k = \lambda_k\mathsf{M}\boldsymbol{u}_k$, where $\boldsymbol{u}_k$ is the k-th eigenvector in U corresponding to λ_k.

We obtain:

$$\frac{\partial\mathsf{K}}{\partial p_j}\boldsymbol{u}_k + K\frac{\partial\boldsymbol{u}_k}{\partial p_j} = \lambda_k\mathsf{M}\frac{\partial\boldsymbol{u}_k}{\partial p_j} + \lambda_k\frac{\partial\mathsf{M}}{\partial p_j}\boldsymbol{u}_k + \frac{\partial\lambda_k}{\partial p_j}\mathsf{M}\boldsymbol{u}_k. \tag{6}$$

Rearranging Equation (6) gives:

$$(\mathsf{K} - \lambda_k\mathsf{M})\frac{\partial\boldsymbol{u}_k}{\partial p_j} + \left(\frac{\partial\mathsf{K}}{\partial p_j} - \lambda_k\frac{\partial\mathsf{M}}{\partial p_j}\right)\boldsymbol{u}_k = \frac{\partial\lambda_k}{\partial p_j}\mathsf{M}\boldsymbol{u}_k. \tag{7}$$

Pre-multiplying both sides by $\boldsymbol{u}_i^T$ gives the derivative of eigenvalues:

$$\frac{\partial\lambda_k}{\partial p_j} = \boldsymbol{u}_k^T\left(\frac{\partial\mathsf{K}}{\partial p_j} - \lambda_k\frac{\partial\mathsf{M}}{\partial p_j}\right)\boldsymbol{u}_k. \tag{8}$$

Here, the derivatives $\frac{\partial\mathsf{K}}{\partial p_j}$ and $\frac{\partial\mathsf{M}}{\partial p_j}$ of mass and stiffness matrices depend on the specific material models and shape parameterizations.

For simple examples such as those in §9, we are able to analytically compute the derivatives of K and M matrices using symbolical derivatives provided in such commercial packages as Matlab and Mathematica. For complex geometries or material models, we simply use finite difference to estimate the derivative values. As a result, this derivative formula is general to different parameterizations while retaining the efficiency.

5 Derivative of Generalized Eigenvectors

If the desired modal vibration amplitudes are a^*, we need to solve the nonlinear optimization problem to minimize the energy function (4). The derivative of this energy is related to the derivative of generalized eigenvectors with respect to the shape parameters $\boldsymbol{p}$. In particular, we have:

$$\frac{\partial E_a}{\partial p_j} = 2\sum_{k\in\mathcal{K}_a}\frac{w_k}{\bar{a}_1}\left[a_k(\boldsymbol{p}) - a_k^*\right]\boldsymbol{f}^T\frac{\partial\boldsymbol{u}_k}{\partial p_j}.$$

Therefore, core to this computation is the evaluation of $\frac{\boldsymbol{u}_k}{\partial p_j}$. Similar to optimizing the eigenvalues, we start from Equation (7) and notice that:

$$\mathsf{K} - \lambda_k\mathsf{M} = \mathsf{U}^{-T}(\Lambda - \lambda_k I)\mathsf{U}^{-1}, \tag{9}$$

and its pseudo inverse (Moore-Penrose inverse) can be expressed as:

$$(\mathsf{K} - \lambda_k\mathsf{M})^+ = \mathsf{U}(\Lambda - \lambda_k I)^+\mathsf{U}^T. \tag{10}$$

Next, we notice that:

$$(\mathsf{K} - \lambda_k\mathsf{M})^+(\mathsf{K} - \lambda_k\mathsf{M}) = I - \boldsymbol{u}_k\boldsymbol{u}_k^T\mathsf{M}, \tag{11}$$

and also:

$$(\mathsf{K} - \lambda_k\mathsf{M})^+\mathsf{M}\boldsymbol{u}_k = (\mathsf{U}(\Lambda - \lambda_k I)^+)_k = 0. \tag{12}$$

Pre-multiplying the pseudo inverse $(\mathsf{K} - \lambda_k\mathsf{M})^+$ on both sides of Equation (7) yields:

$$(I - \boldsymbol{u}_k\boldsymbol{u}_k^T M)\frac{\partial\boldsymbol{u}_k}{\partial p_j} = -(\mathsf{K} - \lambda_k\mathsf{M})^+\left(\frac{\partial\mathsf{K}}{\partial p_j} - \lambda_k\frac{\partial\mathsf{M}}{\partial p_j}\right)\boldsymbol{u}_k. \tag{13}$$

Finally, differentiating $\boldsymbol{u}_k^T\mathsf{M}\boldsymbol{u}_k = 1$, we have:

$$\boldsymbol{u}_k^T\frac{\partial\mathsf{M}}{\partial p_j}\boldsymbol{u}_k = -2\boldsymbol{u}_k^T\mathsf{M}\frac{\partial\boldsymbol{u}_k}{\partial p_j}. \tag{14}$$

Substituting this expression in Equation (13), we receive:

$$\frac{\partial\boldsymbol{u}_k}{\partial p_j} = -(\mathsf{K} - \lambda_k\mathsf{M})^+\left(\frac{\partial\mathsf{K}}{\partial p_j} - \lambda_k\frac{\partial\mathsf{M}}{\partial p_j}\right)\boldsymbol{u}_k + \frac{1}{2}\left(\boldsymbol{u}_k^T\frac{\partial\mathsf{M}}{\partial p_j}\boldsymbol{u}_k\right)u_k. \tag{15}$$

Again, this formula involves the derivative of mass and stiffness matrices with respect to the parameters, as well as the pseudo-inverse of $(\mathsf{K} - \lambda_k\mathsf{M})$. They all can be numerically computed or analytically computed when symbolic derivatives are derivable.

6 Free Vibration with Stands

We detail how our stand creation algorithm chooses support vertices. The method has three steps: determining candidate supporting vertices, sorting vertices based on their potential to induce damping in desired or undesired frequencies and selecting a concrete subset of these vertices to support the object.

Support Locations. We initialize the set of candidate vertices, $\mathcal{V}_c$, with all object vertices that are in contact with the ground when our object is in its playable orientation. We define the playable orientation as the orientation in which the object is upright and its contact patch is easily accessible. In our case, this playable orientation is known *a priori*. Our goal is to select support vertices, $\mathcal{V}_s$, from $\mathcal{V}_c$ such that our object is stable and has optimal sound quality. We define stability in the traditional sense: the center of mass of the object and its contact patch are inside the convex hull of the support vertices. We optimize sound quality by minimally damping the desired vibrational frequencies while simultaneously attempting to maximally damp all undesired frequencies. In the main paper, Figure 5 shows an example of the optimal placement of support vertices.

A frequency is damped if its modal shape is not allowed to vibrate as if it were free. This tells us that ideal support vertices have small maximum displacements in all desired frequencies and large minimum displacements in all undesired frequencies. In our case, we find a reasonable set of support vertices using an efficient 1D search.

Let $\mathcal{S} = \left\{S^1, \ldots, S^M\right\}, S^k \in \mathcal{R}^N$ be the set of object vibration modes (i.e., eigenvectors of Equation (1)). Here N is the number of vertices in the tetrahedral simulation mesh. We denote the displacement of the i^{th} candidate vertex in the k^{th} mode as $s_i^k \in \mathcal{R}^3$. Furthermore let $\mathcal{J} = \{1, \ldots, M\}$ be the indices of our user-defined frequencies. Our goal is to select $\mathcal{V}_s$ such that $\max\left(s_i^j\right)$ is small and $\min\left(s_i^l\right)$ is large $\forall \boldsymbol{v}_i \in \mathcal{V}_s$, $\forall j \in \mathcal{J}$ and $\forall l \notin \mathcal{J}$.

We build two sorted lists of vertices, $\mathcal{F}$ and $\mathcal{D}$. $\mathcal{F}$ is the free-vibration list. We insert all $\boldsymbol{v}_i \in \mathcal{V}_c$ into this list and sort them in ascending order of $\max\left(\frac{s_i^j}{s^{j*}}\right)$ where s^{j*} is the maximum vertex displacement for the j^{th} user-desired mode. Conversely $\mathcal{D}$ is the damping list. Into this list we insert all $\boldsymbol{v}_i \in \mathcal{V}_c$ and sort them in descending order of $\min\left(\frac{s_i^l}{s^{l*}}\right)$ where s^{l*} is the maximum vertex displacement for the l^{th} undesired mode. We now filter $\mathcal{F}$ and $\mathcal{D}$ using a scalar threshold t, rejecting candidate vertices in $\mathcal{F}$ with cost above t as well as vertices in $\mathcal{D}$ with cost below t. The remaining vertices form $\mathcal{V}_s$. We perform a 1D binary search for t such that $|\mathcal{V}_s|$ is minimized and our stability criterion are met.

References

BICKEL, B., BÄCHER, M., OTADUY, M. A., MATUSIK, W., PFISTER, H., AND GROSS, M. 2009. Capture and modeling of non-linear heterogeneous soft tissue. *ACM Trans. Graph. 28*, 3 (July).

BICKEL, B., BÄCHER, M., OTADUY, M. A., LEE, H. R., PFISTER, H., GROSS, M., AND MATUSIK, W. 2010. Design and fabrication of materials with desired deformation behavior. *ACM Trans. Graph. 29*, 4 (July), 63:1–63:10.

COMSOL, A. 2005. Comsol multiphysics user's guide. *Version: September*.

DE LEEUW, J. 2007. Derivatives of generalized eigen systems with applications. Tech. rep., UCLA Department of Statistics.

HUGHES, T. J. R. 2012. *The Finite Element Method: Linear Static and Dynamic Finite Element Analysis*. Dover Civil and Mechanical Engineering. Dover Publications.

O'BRIEN, J. F., SHEN, C., AND GATCHALIAN, C. M. 2002. Synthesizing sounds from rigid-body simulations. SCA '2002, 175–181.

Shapeways. `https://www.shapeways.com/materials/steel`. Accessed: 2014-12-31.